



Electrochemical behavior of a thermally prepared RuO₂ anode at different temperatures

KAMBIRE Ollou^{1*}, BERTE Mohamed², GNAMBA Corneil Quand-Même², KOUYA Tyeoula Monnequimond Arnaud², KOFFI Konan Sylvestre², KIMOU Kouakou Jocelin², OUATTARA Lassiné^{2**}

¹UFR Sciences et Technologies, Université de Man, BP 20 Man, Côte d'Ivoire

²Laboratoire de constitution et réaction de la matière, UFR SSMT, Université Félix Houphouët-Boigny de Cocody, Abidjan, 22 BP 582 Abidjan 22, Côte d'Ivoire

*Corresponding author, Email address: kambireollo@yahoo.fr

**Corresponding author, Email address: ouatlassine@yahoo.fr

Received 08 Feb 2025,
Revised 12 June 2025,
Accepted 20 June 2025

Keywords:

- ✓ Electrode;
- ✓ RuO₂;
- ✓ Temperature;
- ✓ Voltammogram;
- ✓ Voltammetric charge

Citation: Kambire O., Berte M., Gnamba C.Q.-M., Kouya T.M.A., Koffi K.S., Kimou K.J., Ouattara L. (2025) Electrochemical behavior of a thermally prepared RuO₂ anode at different temperatures, *J. Mater. Environ. Sci.*, 15(7), 1324-1337

Abstract: The preparation temperature of an electrode strongly influences its electrochemical behavior. Thus our objective is to study the influence of the calcination temperature of RuO₂ on its electrochemical behavior. In this work, the RuO₂/Ti electrodes used were prepared thermally at 400 °C, 600 °C or 750 °C using brushes from diluted RuCl₃.xH₂O precursor solutions in isopropanol. Characterization by scanning electron microscopy confirms the presence of overlapping layers of ruthenium oxide, cracks and some pores. The characterization of these electrodes by X-ray diffraction confirmed the presence of RuO₂ on their surfaces. The crystallinity of RuO₂ increases with temperature and a mixture of two forms of ruthenium oxide is noted for the electrode prepared at 750°C. The electrochemical characterization showed that the prepared electrodes are porous. The electrode prepared at 600°C has the highest voltammetric charge. It is also noted that the electrode prepared at 600°C has the highest number of active sites. The study of the ferri-potassium ferrocyanide couple showed a quasi-reversible behavior of the on all the prepared electrodes.

1. Introduction

Since the Volta cell, electrochemistry has developed enormously, both at the fundamental level and in terms of its application in various sectors: energy (production and storage), electrosynthesis, study of corrosion phenomena, preparation of reactive metals or non-metals, analysis, or even the world of life (Aly *et al.*, 2025; Laouini *et al.*, 2025; Diaz-Ramos *et al.*, 2023; Kambiré *et al.*, 2021 & 2022a; Koffi *et al.*, 2021; Hmamou *et al.*, 2013). The strength of electrochemistry lies in its multidisciplinary (Aichouch *et al.*, 2025; Alkhadra *et al.*, 2022). As a result, it is continuously exploring new applications in various fields such as the treatment of urban wastewater, industrial wastewater, agricultural wastewater, hospital wastewater or more recently wastewater from the petrochemical industry

(AlJaberi *et al.*, 2023; Batool et Zafar, 2025; Tran et Pham, 2023; Kambiré *et al.*, 2022b; Kouadio *et al.*, 2021; Errami *et al.*, 2013), since biological treatments are becoming impotent when faced with refractory or recalcitrant molecules (Boutourda *et al.*, 2025; Sadia *et al.*, 2021; Zhu *et al.*, 2023; Bar-Niv *et al.* 2022; Dutta *et al.*, 2024). However, this technique implies the choice of the electrode to be used as anode (Antonini *et al.*, 2025; Tao *et al.*, 2024; Fdez-Sanromán *et al.*, 2024). The RuO₂ electrode is the preferred candidate because it has good oxygen evolution kinetics and its lifetime easily exceeds five years under industrial operating conditions (Kambire *et al.*, 2015a & 2020a).

In addition to oxygen production, ruthenium oxide is used in many other fields. In industry, it is used in catalysis for various reactions such as ammonia production, acetic acid production from N-heterocycles and alcohol oxidation (Ding *et al.*, 2025). It is used in electrocatalysis for the production of chlorine, chlorine oxide and oxygen (Zhang *et al.*, 2025), titanium coating in the electrolytic production of chlorine, chlorate and caustic (Lu *et al.*, 2025). Ruthenium oxide is also used in stable deacon process, in electronics, Solar Cells, Biomedical Applications, Sensors, Jewelry and Alloys, Binder for cemented carbides (Liu *et al.*, 2025; Li *et al.*, 2025).

The use of ruthenium oxide anodes in electrochemistry involves them in reaction processes where the surface of the electrode through the electrode/electrolyte interface, participates enormously. Several studies have been carried out at the electrode/electrolyte interface in order to elucidate the reaction mechanisms taking place at this interface due to its complexity (Ollo *et al.*, 2020; Kambiré *et al.*, 2015b & 2020a; Appia *et al.*, 2016). Similarly, to determine the structure of the electrodes involved in the reaction processes, physical methods such as scanning electron microscopy and X-ray diffraction are generally used (Subramaniyan *et al.*, 2025; Achache *et al.*, 2025; Kambiré *et al.*, 2015c & 2021; Begum *et al.*, 2022 ; Wafia et Samir, 2021 ; Kezhong *et al.*, 2024).

The interest in the development of new electrodes, the surface structure determination and the study of their electrochemical behavior through a simple voltammetric method have motivated this work. The aim of this work is to prepare RuO₂ electrodes by thermal process at different temperatures and to study the influence of temperature on their electrochemical behavior. This study will be carried out using cyclic voltammetries.

2. Methodology

The electrodes used in the following work were all prepared in our laboratory with appropriate metallic precursors. The coating precursors were prepared from RuCl₃·xH₂O (Fluka). All the precursors were dissolved in pure isopropanol (Fluka) used as solvent. The commercial products were used as received without any further treatment.

The titanium substrates on which the electrode films were deposited have the following dimension 1.6 × 1.6 × 0.5 cm. The surface of each substrate was sandblasted to ensure good adhesion of the deposit on it. After, sandblasting, all the substrates were washed vigorously in water and then in isopropanol to clean their surface from residual sands. The substrates were then dried in an oven at 80°C and weighed. After that, the precursor was applied by a painting procedure on the titanium (Ti) substrate then put in an oven for 15 min at 80 °C in air to allow the solvent evaporation (Kambire *et al.*, 2015a & 2015c). Then after, it is put in a furnace at 400 °C, 600°C or 750°C for 15 min in air to allow the decomposition of the precursor. These steps were repeated until the desired mass of the coating is reached. A final decomposition of 1 h was done at 400 °C, 600°C or 750°C.

The voltammetric measurements were performed on the prepared electrodes in a three-electrode electrochemical cell using an Autolab PGStat 20 (Ecochemie). The electrodes used consist of the working electrode (prepared material), a platinum counter electrode (wound platinum wire) and the

reference electrode (RE) was a saturated hydrogen electrode (SHE). To overcome the potential ohmic drop, the reference electrode was mounted in a luggin capillary and placed close to the working electrode by a distance of 1 mm. The apparent exposed area of the working electrode was 1 cm² (Kambire *et al.*, 2015a & 2015c).

Products such as KClO₄ (Prolabo), H₂SO₄ (Suprapur Merck), NaOH (Prolabo), K₃Fe(CN)₆ (Fluka) and K₄Fe(CN)₆ (Fluka) were used as received. All the solutions used in the current work have been prepared with distilled water. All the electrochemical experiments were made at ambient temperature of 25 °C (Kambire *et al.*, 2015b).

3. Results and Discussion

3.1. Physical characterization of the electrodes

3.1.1. Scanning electron microscopy (SEM) analysis

The morphology characterization of the titanium substrates and the thermally prepared electrodes at the temperatures of 400°C, 600°C and 750°C was performed by SEM microphotos analysis. The results obtained are presented in **Figure 1**.

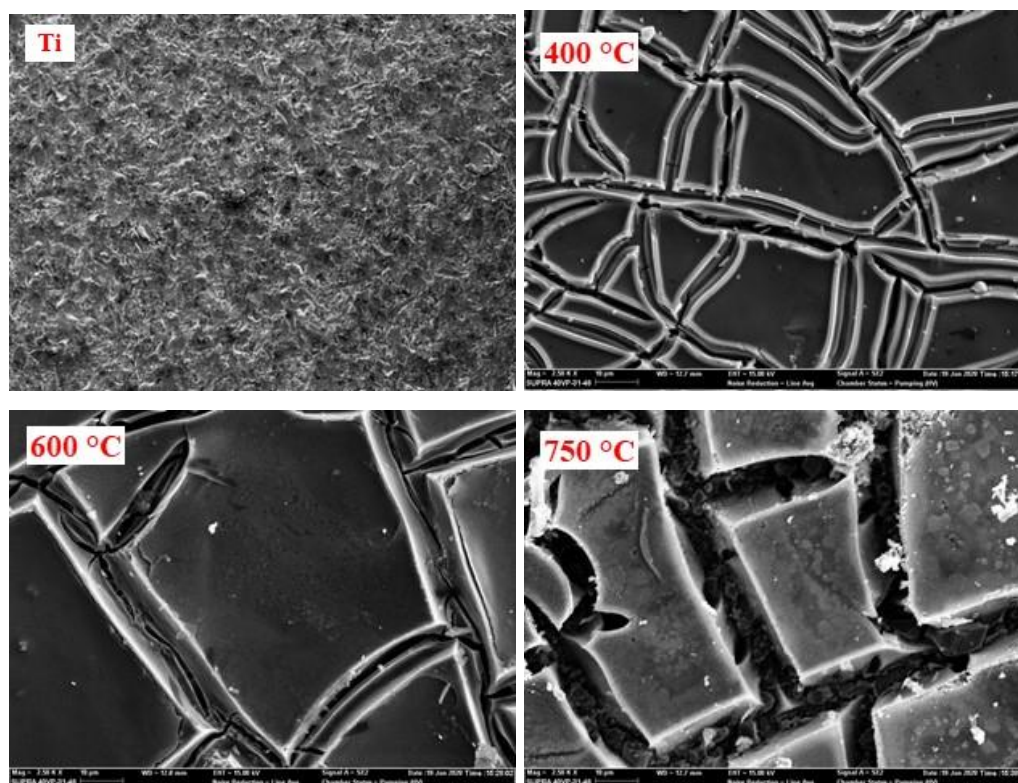


Figure 1. SEM microphotos of RuO₂ electrodes

These microphotos show overlapping layers of ruthenium oxide, cracks and a few pores in accordance with the literature (Kambire *et al.*, 2015a ; Appia *et al.*, 2016 ; Pohan *et al.*, 2020). The cracks observed on the ruthenium oxide surface occur during the cooling of the deposit due to the mechanical stresses produced by the difference in the thermal expansion coefficients of the substrate and the deposit (Kambire *et al.*, 2015b).

3.1.2. Analysis of the electrodes by XRD

The electrodes surfaces were analyzed by X-ray diffraction. The results obtained are shown in **Figure 2**. This figure shows that at 400°C and 600°C, the peaks are at the same 2θ angle. The peaks are thinner at 600°C compared to 400°C. The position of these peaks is characteristic of rutile-type RuO_2 . The crystallinity of RuO_2 increases with temperature. This is confirmed with the fineness of the peaks at 750°C. Additional peaks are observed at 750°C. The presence of these peaks suggests a change in the nature of the RuO_2 film. A mixture probably of two forms of ruthenium oxide.

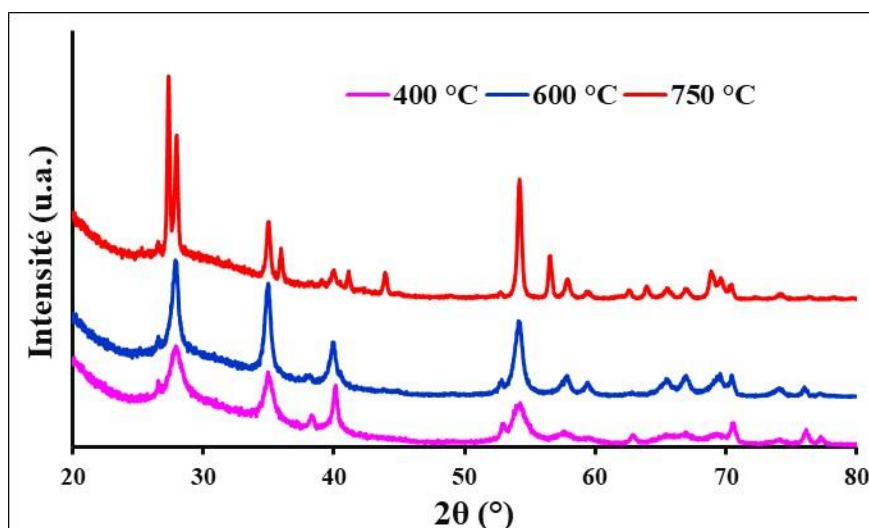


Figure 2. X-ray spectra of the electrodes

3.2 Electrochemical characterization of the electrodes

3.2.1. Electrochemical behavior of the electrodes in ferri/ferrocyanide redox couple

The electrochemical behavior of the ferri/ferrocyanide redox couple was studied on the prepared electrodes. **Figure 3** shows the influence of the potential scan rate on the behavior of the electrodes. For each electrode, we note the presence of a peak in the forward potential scan and a peak in the backward potential scan on the voltammograms indicating that an oxidation of the ferrocyanide ion and a reduction of the ferricyanide ion occurs. On these figures we can observe the increase in absolute values of the peak currents with the potential scan rate. The oxidation current peaks have been plotted against the square root of the potential scan rate for all electrodes. The results are presented in **Figure 4**. A linear evolution is observed for all the electrodes indicating that the process is diffusion controlled (Kambire *et al.*, 2015a & 2015c). **Figure 4** also shows that whatever the potential scan rate, the oxidation peaks current of the electrode prepared at 600°C is higher than those of the other electrodes. This clearly shows that the electrode prepared at 600°C is more conductive than the electrodes prepared at 400°C and 750°C (Kambire *et al.* 2015c).

Figure 3 also shows that the anodic peaks potentials increase (move in the increasing direction of potentials) when the potential scan rate increases. It is noted that the cathodic peak potentials decrease (move in the decreasing direction of potentials) when the potential scan rate increases. The potential difference (ΔE_p) between the anodic peak potential and the cathodic peak potential was determined for each potential scan rate ranging from 5 mV/s to 150 mV/s. The results obtained are presented in **Table 1**. This table shows that the potential difference between the

anodic and cathodic peak currents is always greater than 60 mV for all electrodes regardless of the potential scan rate. These results show a quasi-reversible behavior of the ferri/ferrocyanide redox couple on all the electrodes studied (Pohan *et al.*, 2013).

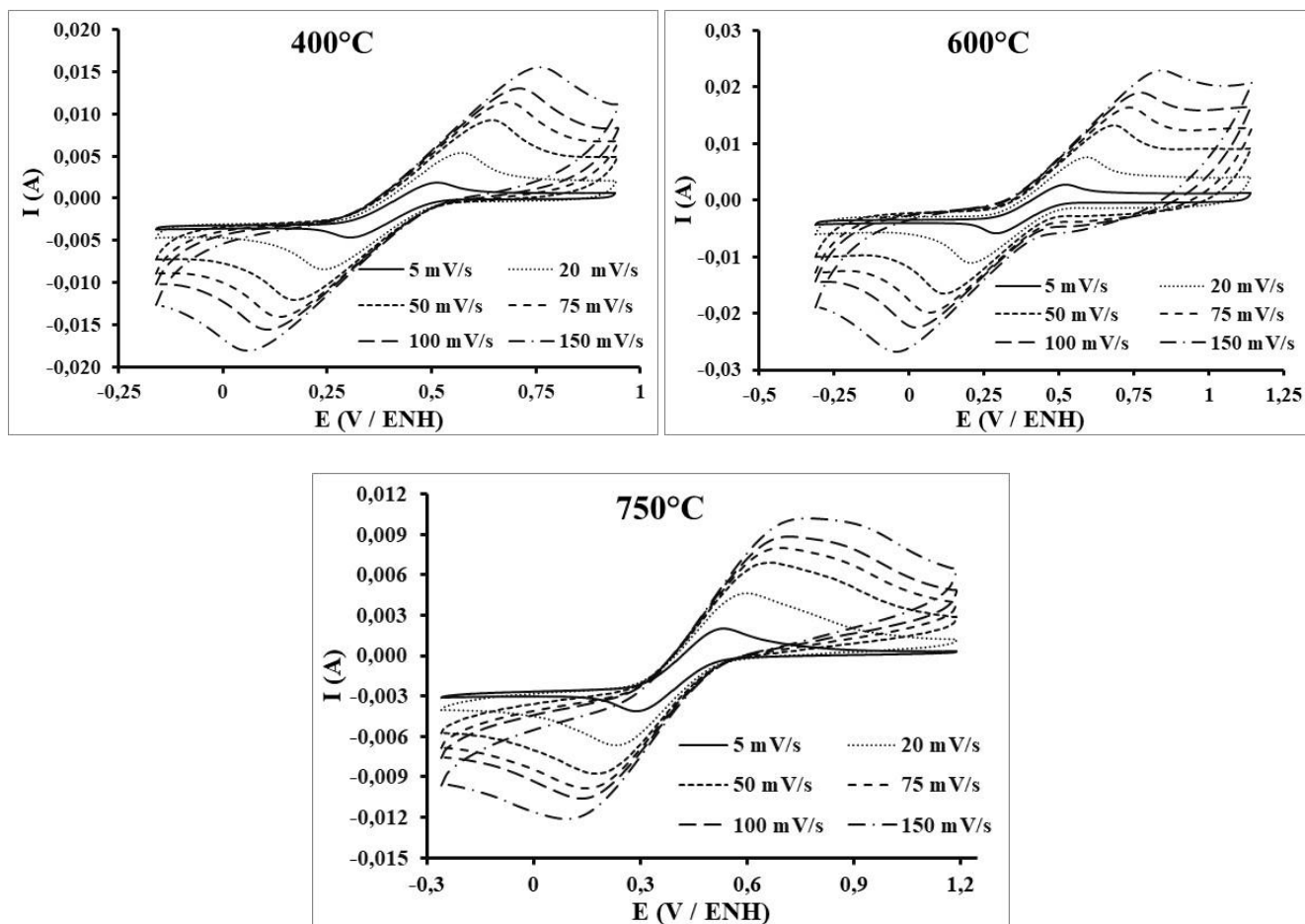


Figure 3. Voltammetric curves at different potential scan rates of the electrodes in the presence of 0.1 M ferri/ferrocyanide redox couple in 0.1 M KClO₄

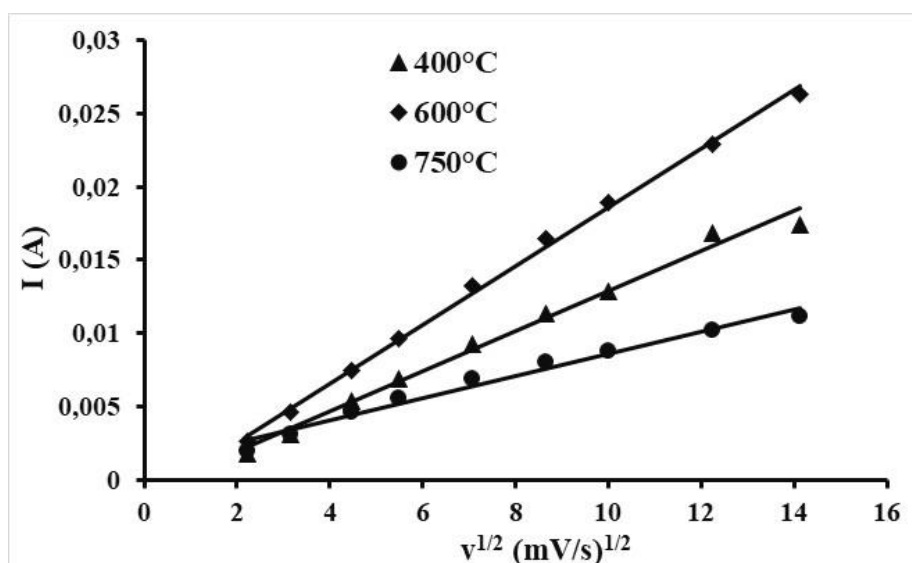


Figure 4. Evolution of anodic peaks current density against the square root of the scan rate for the all electrodes

Table 1. The gap between the peak potentials of the electrodes in 0.1 M ferri/ferrocyanide, supporting electrolyte: KClO₄ 0.1 M

Potential scan rate	ΔE (V)		
	400°C	600°C	750°C
5 mV/s	0.204	0.232	0.238
20 mV/s	0.339	0.393	0.359
50 mV/s	0.493	0.571	0.474
75 mV/s	0.553	0.665	0.538
100 mV/s	0.624	0.755	0.564
150 mV/s	0.670	0.867	0.746

3.2.2. Electrochemical behaviour of electrodes in sulphuric acid

3.2.2.1. Aspect of the voltammograms

The electrochemical characterization of the prepared ruthenium oxide electrodes was performed in 0.5 M sulfuric acid (H₂SO₄). The measurements were performed at 25 mV/s on the prepared electrodes.

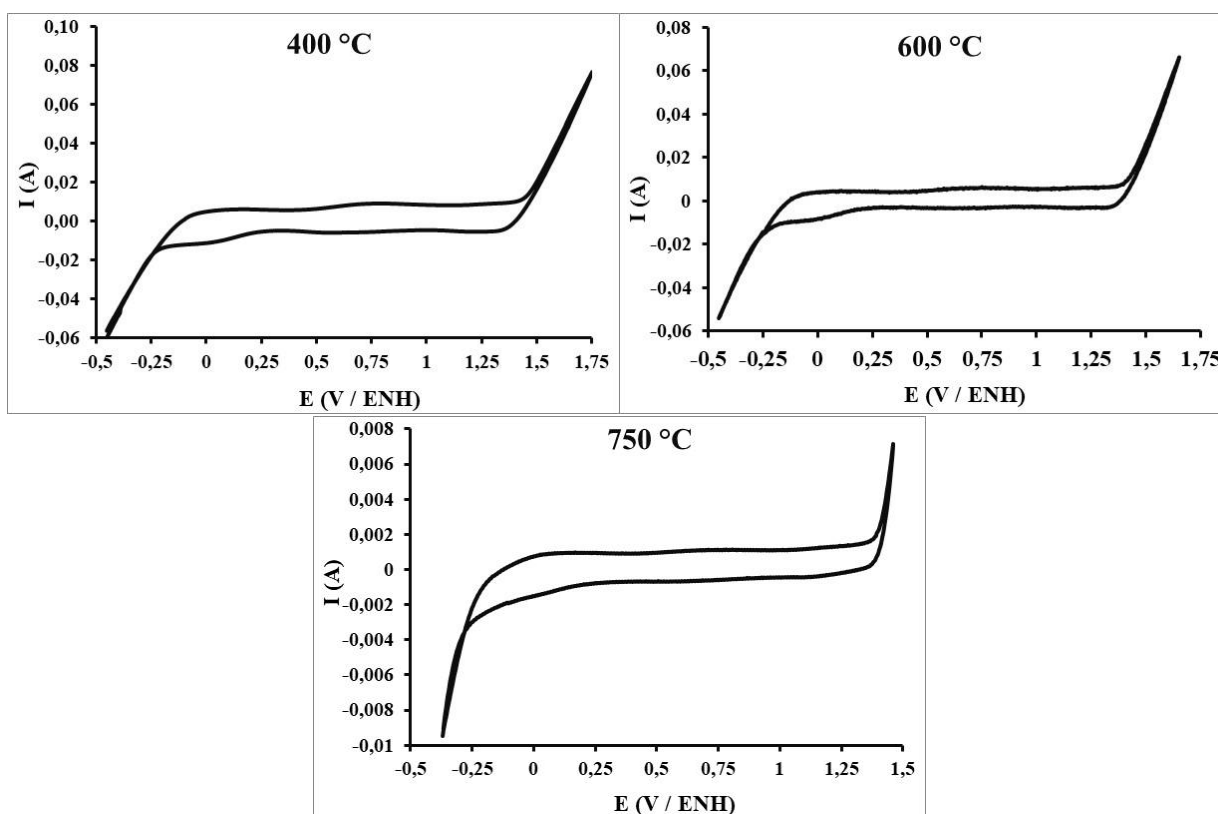


Figure 5. Voltammograms of electrodes in 0.5 M H₂SO₄, $v = 25\text{mV/s}$

Figure 5 gives the appearance of the voltammograms obtained. This figure shows that the electrode prepared at 400°C shows a shoulder at 0.78 V and an oxidation wave at 1.23 V. Hydrogen evolution starts at -0.17 V and oxygen evolution starts at 1.39 V. The stability domain of the supporting electrolyte is $\Delta E = E(\text{O}_2) - E(\text{H}_2) = 1.56$ V. With the electrode prepared at 600°C, we observe a shoulder at 0.69 V and an oxidation wave at 1.19 V. The hydrogen evolution starts at -0.17 V and the oxygen evolution starts at 1.35 V. The stability domain of the supporting electrolyte is equal to 1.52 V. For the 750°C electrode, a shoulder is also observed at 0.75 V and an oxidation wave at 1.13 V.

Hydrogen evolution starts at -0.22 V and oxygen evolution starts at 1.34 V. The stability domain of the supporting electrolyte is 1.56 V. For all 3 electrodes, **Figure 5** shows, in the stability domains of the supporting electrolyte, a strong capacitive charge. It also shows that the anodic and cathodic peaks present are less marked. This weak peak definition is indicative of an inhomogeneous surface and characteristic of thermally prepared DSAs. The peaks and waves observed on the voltammograms can be attributed to the Ru(III)/Ru(IV) and Ru(IV)/Ru(VI) transitions respectively (Wen et Hu, 1992; Rosario et al. 2006).

3.2.2.2. Voltammetric charging of the electrodes in sulfuric acid media

Voltammetric measurements were performed on the different electrodes in their stability domain in 0.5 M H₂SO₄ media at different potential scan rates. The results obtained with the prepared electrodes are presented in **Figure 6**.

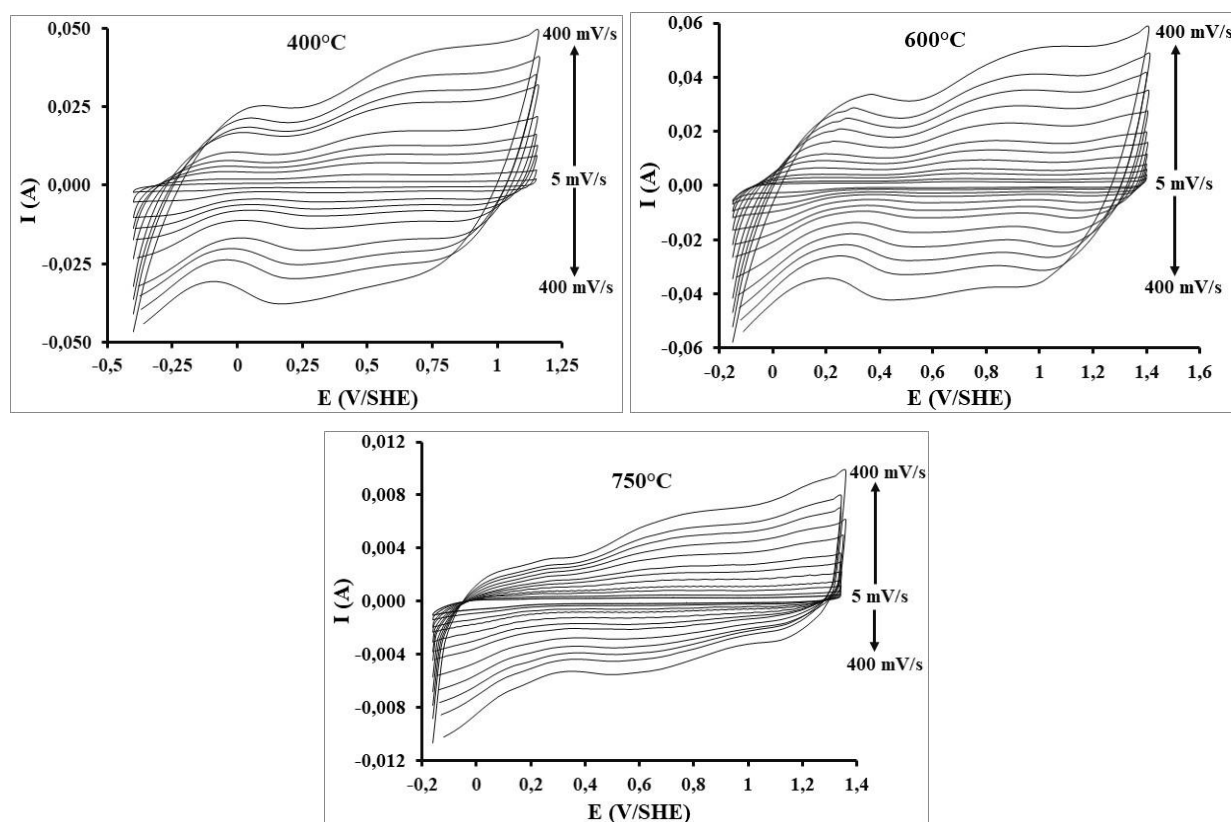


Figure 6. Cyclic voltammograms at different potential scan rates in the stability domain of the supporting electrolyte on the electrodes in 0.5 M H₂SO₄

Figure 6 shows that the general shape of the voltammograms is independent of the potential scan rate. All voltammograms are quasi-symmetric in the potential range explored. Nevertheless, for potential scan rates below 30 mV/s and above 150 mV/s, the appearance of the curves changes significantly. This change is due to the relatively slow phenomena taking place at the surface of the electrodes at low potential scan rates and to the uncompensated ohmic drop in the solution for high potential scan rates. Similar results were obtained with all the prepared electrodes.

The electrochemical activity of ruthenium oxide can be characterized by the voltammetric charge (q) between the H₂ and O₂ evolution reactions. This charge is obtained by integration of the voltammograms areas. This integration led to the determination of the total charges q presented as a

function of the potential scan rate for each of the electrodes in **Figure 7**. The results obtained show that for a given potential scan rate, q varies from one electrode to another. We note that q increases from 400 to 600 °C. Then q decreases when the calcination temperature of the electrodes increases from 600 to 750°C. This shows that there is a change in the nature of the RuO₂ film for temperatures above 600°C. These results indicate that the highest q was obtained with the electrode prepared at 600°C. Whatever the potential scan rate, the decreasing order of voltammetric charges is: $q(600^\circ\text{C}) > q(400^\circ\text{C}) > q(750^\circ\text{C})$.

Figure 7 shows a rapid decrease in voltammetric charges for low scan rates (from 5 mV/s to 30 mV/s). This rapid decay stabilizes at high potential scan rates. The dependence of the voltammetric charges on the scan rate in potential ([Kambiré et al., 2020b](#); [Baronetto et al., 1994](#)) is explained by the fact that there are regions of the surface containing active sites that are less accessible than others. These active sites, which are difficult to access, are progressively accessible as the potential scan rates decrease, which causes an increase in q .

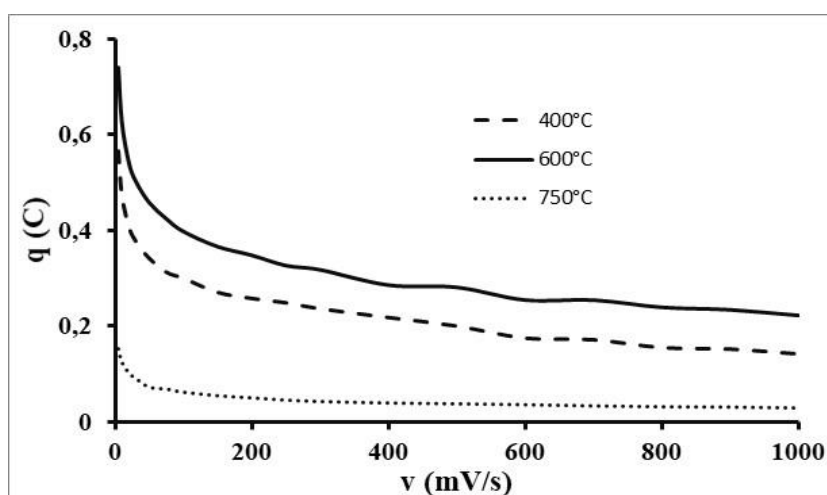


Figure 7. Evolution of the voltammetric charge as a function of the potential scan rate

At high potential scan rates, the various processes are surface phenomena (outer layer), whereas at low potential scan rates the processes take place in the inner and outer layers of the electrodes. By plotting the curves $q = f(v^{-1/2})$ the values of the external charges (q_{ext}) of the electrodes can be determined. The equation $q = f(v^{-1/2})$ is an affine line. Based on the model of Trasatti ([Trasatti, 1991](#)), **Eqn. 1** will allow the determination of the electrode external charge. For an infinite scan rate corresponding to the extreme (largest) value of the potential scan rate, $q(v) = q_{\text{ext}}$ is the intercept.

$$q(v) = q_{\text{ext}} + k_1 v^{-1/2} \quad \text{Eqn. 1}$$

Where: k_1 is a constant; v is the potential scan rate; $q(v)$ is the measured voltammetric charge; $q_{\text{ext}}(v)$ is the external (surface) voltammetric charge.

Only the points that result from high potential scan rates (50 mV/s to 250 mV/s) are used for the determination of external charges with $q_{\text{ext}} \geq 0$.

Plotting the curves $\frac{1}{q(v)} = f(v^{1/2})$ allows determination of the total charges values (q_{tot}) of the electrodes. The equation $\frac{1}{q(v)} = f(v^{1/2})$ is an affine line. For a scan rate corresponding to the scan rate

at zero potential (lower extreme) $\frac{1}{q(V)} = \frac{1}{q_{tot}}$ is the intercept. To obtain the internal charge, Trasatti (Trasatti, 1991) proposed another relation.

$$\frac{1}{q(V)} = \frac{1}{q_{tot}} + k_2 v^{1/2}. \quad \text{Eqn. 2}$$

Where: k_2 is a constant; v is the potential scan rate; $q(v)$ is the measured voltammetric charge; $q_{tot}(v)$ is the total voltammetric charge (surface + internal).

The points corresponding to low scan rate (from 5 mV/s to 30 mV/s) are used for the determination of total charges with $q_{tot} \geq 0$.

In this work, the curves $q(v) = f(v^{-1/2})$ and $\frac{1}{q(V)} = f(v^{1/2})$ were performed for the different prepared electrodes. The curves obtained with the electrode prepared at 400 °C are shown in **Figure 8A** and **8B**. Similar results were obtained with the other electrodes (curves not shown). These curves allowed to determine the internal and external charges of the electrodes. The results obtained are presented in **Figure 9**.

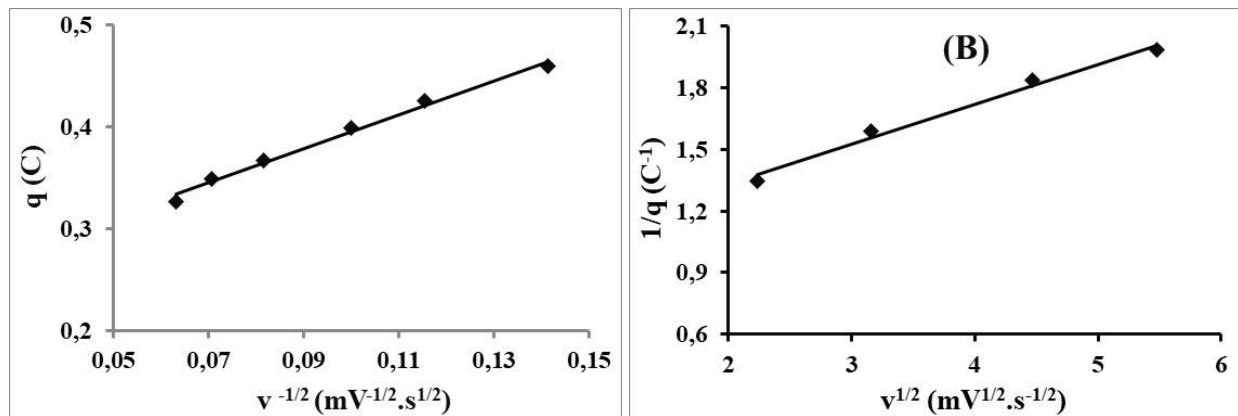


Figure 8. Curves $q(v) = f(v^{-1/2})$ and $\frac{1}{q(V)} = f(v^{1/2})$ performed in 0.5 M H₂SO₄ on the electrode prepared at 600 °C

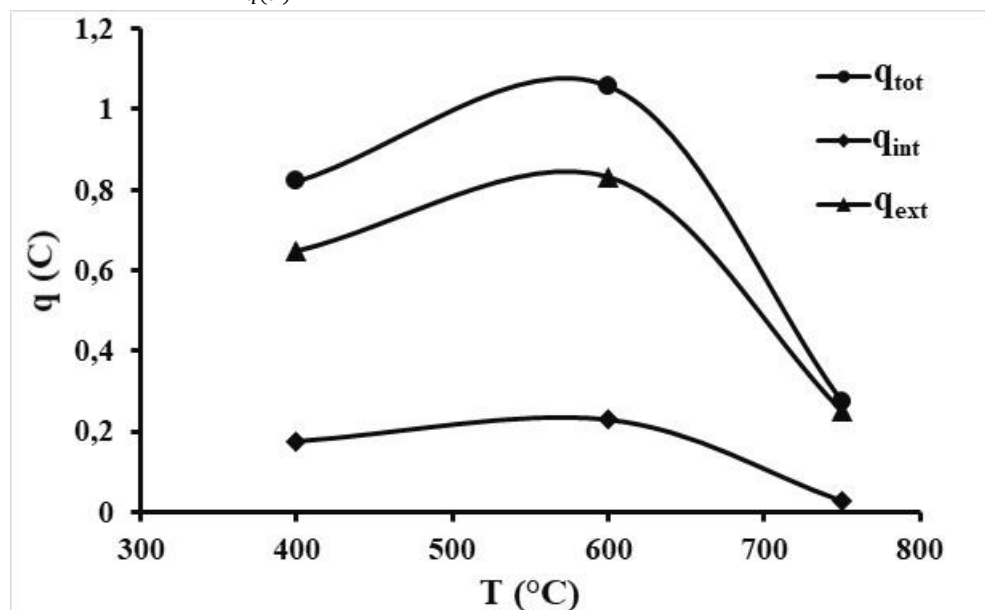


Figure 9. Extrapolated values of charges as a function of temperature

Figure 9 shows the internal, external and total charges of the prepared electrodes. We note that the internal charges are greater than 0 ($q_{\text{int}} > 0$) for all the electrodes prepared. This result allows us to indicate that the prepared electrodes are porous. It appears that the surfaces inside the pores participate in the charging and discharging processes at the electrode/electrolyte solution interface. This figure shows that the internal, external and total charges increase when going from 400 °C to 600 °C and then decrease from 750 °C. This shows that the electrode prepared at 600 °C has the highest number of active sites.

Conclusion

RuO₂/Ti electrodes used in this work were prepared thermally at 400 °C, 600 °C and 750 °C from precursor solutions of RuCl₃.xH₂O in isopropanol. Characterization by scanning electron microscopy confirms the presence of overlapping layers of ruthenium oxide, cracks and some pores. The characterization of these electrodes by X-ray diffraction confirmed the presence of RuO₂ on their surfaces. RuO₂ crystallinity increases with temperature and a mixture of two forms of ruthenium oxide is noted for the electrode prepared at 750°C. The electrochemical characterization showed that the prepared electrodes are porous. The electrode prepared at 600°C has the highest voltammetric charge. It is also noted that the electrode prepared at 600°C has the highest number of active sites. The study of the ferri-potassium ferrocyanide couple showed a quasi-reversible behavior of the on all the prepared electrodes.

Acknowledgement: We greatly thank the Swiss National Funds for its financial support that allowed this work to be carried out. Our Team has received part of the grant IZ01Z0_146919 for that work. We also thank Prof. Bakayoko-Ly Ramata, prior the president of the University Felix Houphouet-Boigny for her help in the realization of that work.

Disclosure statement: *Conflict of Interest:* The authors declare that there are no conflicts of interest.

Compliance with Ethical Standards: This article does not contain any studies involving human or animal subjects.

References

- Achache M., Seddik N.B., Bouchta D., Draoui K., Choukairi M. (2025) NiO nanoparticles modified carbon paste electrode for the voltammetric simultaneous detection of catechol and hydroquinone as environmental pollutants. *Microchemical Journal* 208, 112578. <https://doi.org/10.1016/j.microc.2024.112578>
- Aichouch, I., El Magri, A. & Hammouti, B. (2025) Influence of laser power and scan speed on porosity, microhardness, and corrosion resistance in HCl medium of additively manufactured H13 tool steel. *Prog Addit Manuf* (2025). <https://doi.org/10.1007/s40964-025-01068-7>
- AlJaberi F.Y., Ahmed S.A., Makki H.F., Naje A.S., Zwain H.M., *et al.* (2023) Recent advances and applicable flexibility potential of electrochemical processes for wastewater treatment. *Science of The Total Environment* 867, 161361. <https://doi.org/10.1016/j.scitotenv.2022.161361>
- Alkhadra M.A., Su X., Suss M. E., Tian H., Guyes E. N., Shocron A. N., Conforti K. M., *et al.* (2022). Electrochemical Methods for Water Purification, Ion Separations, and Energy Conversion, *Chemical Reviews*, 122 (16), 13547-13635 <https://doi.org/10.1021/acs.chemrev.1c00396>

- Aly R.A., Alaamer A., Ashira T., Alkhajeh S.N., *et al.* (2025) Chapter 13 - Nanophoto/electrochemistry for green energy production, *Electrochemistry and Photo-Electrochemistry of Nanomaterials*, 427-452, <https://doi.org/10.1016/B978-0-443-18600-4.00014-4>
- Antonini G., Rahman M.M., Brooks C., Santoro D., Muller C., Al-Omari A., Bell K., Pearce J.M. (2025) Portable Solar-Integrated Open-Source Chemistry Lab for Water Treatment with Electrolysis. *Technologies* 13(2):57. <https://doi.org/10.3390/technologies13020057>
- Appia F.T.A., Gnamba C.Q.-M., Kambiré O., Berté M., Sadia S.P., Sanogo I., Ouattara L. (2016) Electrochemical Oxidation of Amoxicillin in Its Commercial Formulation on Thermally Prepared RuO₂/Ti. *J. Electrochem. Sci. Technol.* 7(1), 82-89. <https://doi.org/10.5229/JECST.2016.7.1.82>
- Bar-Niv N., Azaizeh H., Kuc M.E., Azerrad S., Haj-Zaroubi M., Menashe O., Kurzbaum E. (2022) Advanced oxidation process UV-H₂O₂ combined with biological treatment for the removal and detoxification of phenol. *Journal of Water Process Engineering* 48: 102923. <https://doi.org/10.1016/j.jwpe.2022.102923>
- Baronetto D., Krstajić N., Trasatti S. (1994) Reply to “note on a method to interrelate inner and outer electrode areas” by H. Vogt. *Electrochimica Acta.* 39 (16): 2359-2362. [https://doi.org/10.1016/0013-4686\(94\)E0158-K](https://doi.org/10.1016/0013-4686(94)E0158-K)
- Batool M., Zafar M.N. (2025) Synthesis of a BiSbS₃@BiSbO₄/CNH nanocomposite for wastewater treatment and electrochemical application *Mater. Adv.* 6: 224 [DOI: 10.1039/D4MA01017E](https://doi.org/10.1039/D4MA01017E)
- Begum B., Bilal S., Shah A.U.H.A., Röse P. (2022) Synthesis, Characterization and Electrochemical Performance of a Redox-Responsive Polybenzopyrrole@Nickel Oxide Nanocomposite for Robust and Efficient Faraday Energy Storage. *Nanomaterials* 12: 513. <https://doi.org/10.3390/nano12030513>
- Boutourda F.Z., Ouvrard R., Pointot T., Mehdi D., Mesquine F., Tredern É.D., Jauzein V. (2025) A continuous-time LPV models for a biofiltration process in wastewater nitrification — A global approach methodology for parametric estimation. *Journal of Process Control* 146: 103356. <https://doi.org/10.1016/j.jprocont.2024.103356>
- Diaz-Ramos M., Roche V., Song R., Fan H., Bureau C., Lepretre J.C. (2023) Electrochemical Impedance Spectroscopy (EIS) of parylene coated magnesium stents in organic solvent to study early corrosion control. *Corrosion Science* 213: 110932.
- Ding L., Zhong B., Kong X., Wang L., Li C., Du Q., Liu C., Sun W. (2025) Sustainable catalytic hydrogenation of high concentration nitrate to ammonia over Ruthenium-based catalysts. *Separation and Purification Technology* 354 (8) : 129275. <https://doi.org/10.1016/j.seppur.2024.129275>
- Dutta L., Sethi G.K., Dey S. (2024) A Comprehensive and Critical Assessment on the Efficiency of Natural and Synthetic Adsorbents for the Removal of Recalcitrant Malachite Green from Water: Present Level and Future Perspectives. *Korean J. Chem. Eng.* 41: 589–607. <https://doi.org/10.1007/s11814-024-00114-4>
- Errami M., Salghi R., Zarrouk A., Zougagh M., Zarrok H., Hammouti B., Al-Deyab S.S. (2013) Electrochemical Treatment of Wastewater Industrial Cartons, *Int. J. Electrochem. Sci.*, 8 N°12, 12672-12682
- Fdez-Sanromán A., Pazos M., Rosales E., Sanromán M.Á. (2024) Advancing in wastewater treatment using sustainable electrosorbents *Current Opinion in Electrochemistry* 44: 101450. <https://doi.org/10.1016/j.coelec.2024.101450>

- Hmamou D. B., Salghi R., Zarrouk A., Aouad M.R., *et al.* (2013), Weight loss, electrochemical, quantum chemical calculations and molecular dynamics simulation studies on 2-(benzylthio)-1,4,5-triphenyl-1H-imidazole as inhibitor for carbon steel corrosion in hydrochloric acid, *Ind. Eng. Chem. Res.*, 52 N°40, 14315-14327. <https://doi.org/10.1021/ie401034h>
- Kambire O., Appia F.T.A., Ouattara L. (2015a) Oxygen and chlorine evolution on ruthenium dioxide modified by platinum in acid solutions. *Revue Ivoirienne des Sciences et Technologie* 25: 21 – 33.
- Kambire O., Pohan L.A.G., Appia F.T.A., Gnamba C.Q.-M., Kondro K.H., Ouattara L. (2015b) Influence of various metallic oxides on the kinetic of the oxygen evolution reaction on platinum electrodes. *J. Electrochem. Sci. Eng.* 5(2): 79-91. <https://doi.org/10.5599/jese.157>
- Kambire O., Pohan L.A.G., Appia F.T.A., Ouattara L. (2015c) Anodic Oxidation of Chlorides on Platinum Modified by Metallic Oxides. *International Journal of Pure and Applied Sciences and Technology* 27(1): 27-43.
- Kambiré O., Pohan L.A.G., Sadia S.P., Kouadio K.E., Ouattara L. (2020a) Voltammetric study of formic acid oxidation via active chlorine on IrO₂/Ti and RuO₂/Ti electrodes. *Mediterranean Journal of Chemistry* 10(8): 799-808. <https://doi.org/10.13171/mjc10802010271525ko>
- Kambiré O., Pohan L.A.G., Kouakou Y.U., Kimou K.J., Koffi K.S., Kouadio K.E., Ouattara L. (2020b) Influence of the coupling of IrO₂ and PtOx on the charging / discharging process at the electrode / electrolytic solution interface. *International Journal of Innovation and Applied Studies* 31 (3): 655-667.
- Kambiré O., Alloko K.S.P., Pohan L.A.G., Koffi K.S., Ouattara L. (2021) Electrooxidation of the Paracetamol on Boron Doped Diamond Anode Modified by Gold Particles. *International Research Journal of Pure & Applied Chemistry* 22(4), 23-35. DOI: [10.9734/irjpac/2021/v22i430401](https://doi.org/10.9734/irjpac/2021/v22i430401)
- Kambiré O., Sadia S.P., Kouakou Y.U., Pohan L.A.G., Koffi K.S., Kouadio K.E., Kimou K.J., Koné S., Ouattara L. (2022a) Kinetic of the Oxygen and Chlorine Evolution Reaction on Platinum Electrodes at Neutral pH. *Asian Journal of Research in Chemistry* 15 (3): 213-219. DOI: [10.52711/0974-4150.2022.00037](https://doi.org/10.52711/0974-4150.2022.00037)
- Kambiré O., Pohan L.A.G., Konan K.F., Berté M., Gnamba C.Q.-M., Ouattara L. (2022b) Behavior of boron-doped diamond anode on methyl orange oxidation. *Journal of Materials and Environmental Science* 13 (11): 1264-1277.
- Kezhong W., Hui Z., Feifei N., Zejin W., Ping L., Mingxing W. (2024) Copper tungstates directly derived from polyoxotungstate-MOF as counter electrodes for dye-sensitized solar cells. *Journal of Industrial and Engineering Chemistry* 130: 648-656. <https://doi.org/10.1016/j.jiec.2023.10.018>
- Koffi K.S., Kambiré O., Kouadio K.E., Kimou K.J., Ouattara L. (2021) Detection of Lead (II) on a Boron-doped Diamond Electrode by Differential Pulse Anodic Stripping Voltammetry. *Chemical Science International Journal* 30 (7): 33-46. DOI: [10.9734/CSJI/2021/v30i730242](https://doi.org/10.9734/CSJI/2021/v30i730242)
- Kouadio K.E., Kambiré O., Koffi K.S., Ouattara L. (2021) Electrochemical oxidation of paracetamol on boron-doped diamond electrode: analytical performance and paracetamol degradation. *Journal of Electrochemical Science and Engineering* 11(2), 71-86. DOI: <https://doi.org/10.5599/jese.932>

- Laouini E., Moukhliiss Y., Oukhrib R., Kachbou Y., Ait Albrimi Y., *et al.* (2025) Synthesis, characterization, and electrochemical performance of amorphous and crystalline FePO₄ used as cathode materials in aqueous Lithium-ion electrolyte, *Mor. J. Chem.*, 13(1), 205-229
- Li Y., Muhammad F., Chen X., Gu D., Li W., Tang J., Cheng M., Du J., Qiao S., *et al.* (2025) Smart multifunctional Cu₂O@RuO₂ nanozyme for angiogenesis and osteogenesis in periodontitis. *Nano Today* 61, 102624. <https://doi.org/10.1016/j.nantod.2024.102624>
- Liu J., Dong F., Huang Y., Fu Y., Lu X., Ma R., Zhang F., Wang S., Zhu W. (2025) Ce-doped TiO₂ supported RuO₂ as efficient catalysts for the oxidation of HCl to Cl₂. *Journal of Environmental Sciences* 149, 234-241. <https://doi.org/10.1016/j.jes.2024.01.017>
- Liu Y., Wang Y., Li H., Kim M.G., Duan Z., Talat K., *et al.* (2025) Effectiveness of strain and dopants on breaking the activity-stability trade-off of RuO₂ acidic oxygen evolution electrocatalysts. *Nat Commun* 16, 1717. <https://doi.org/10.1038/s41467-025-56638-8>
- Lu Y., Jia L., Yang D., Leng Y., *et al.* (2025) Application and localized corrosion of ruthenium oxide-coated titanium anode plates for a 10 kW fuel cell stack under dynamic load cycling. *Journal of Power Sources*, 641, 236838. <https://doi.org/10.1016/j.jpowsour.2025.236838>
- Melliti W., Errami M., Salghi R., Zarrouk A., Bazzi Lh., *et al.* (2013), Electrochemical Treatment of Aqueous Wastes Agricole Containing Oxamyl By BDD-Anodic Oxidation, *Int. J. Electrochem. Sci.*, 8 N°9, 10921-10931
- Ollo K., Lemeyonouin A.G.P., Konan H.K., Lassiné O. (2020) Study of oxygen evolution reaction on thermally prepared $x\text{PtO}_y-(100-x)\text{IrO}_2$ electrodes. *Journal of Electrochemical Science and Engineering*, 10 (4), 347-360. DOI: <https://doi.org/10.5599/jese.806>
- Pohan A.L.G., Ouattara L., Kondro K.H., Kambiré O., Trokourey A. (2013) Electrochemical Treatment of the Wastewaters of Abidjan on Thermally Prepared Platinum Modified Metal Oxides Electrodes. *European Journal of Scientific Research*. 94 (1): 96-108.
- Pohan L.A.G., Kambiré O., *et al.* (2020) Study of lifetime of Platinum Modified Metal Oxides Electrodes. *Int. J. Biol. Chem. Sci.* 14(4), 1479-1488. <https://doi.org/10.4314/ijbcs.v14i4.25>
- Rosario A.V., Bulhões L.O.S., Pereira E.C. (2006) Investigation of pseudocapacitive properties of RuO₂ film electrodes prepared by polymeric precursor method, *Journal of Power Sources*, 158, 795–800.
- Sadia S.P., Kambiré O., Gnamba C.Q.-M., Pohan L.A.G., Berté M., Ouattara L. (2021) Mineralization of Wastewater from the Teaching Hospital of Treichville by a Combination of Biological Treatment and Advanced Oxidation Processes. *Asian Journal of Chemical Sciences* 10 (2): 1-10. DOI: [10.9734/ajocs/2021/v10i219086](https://doi.org/10.9734/ajocs/2021/v10i219086)
- Subramaniyan S., Govindasamy M., Sakkarapani S., Kuo C.-Y. (2025) Exploration of CeO₂ decorated on MoO₃ as a potential electrode for high performance hybrid supercapacitors. *Journal of Alloys and Compounds* 1013: 178518. <https://doi.org/10.1016/j.jallcom.2025.178518>.
- Tao G., Xiang C., Lifeng Y. (2024) Recent advancements in modified SnO₂-Sb electrodes for electrochemical treatment of wastewater. *Journal of Materials Chemistry A*, 12: 4397-4420. <https://doi.org/10.1039/D3TA07238J>
- Tran L.L., Pham T.K.N. (2023) Fabrication of high performance Ti/SnO₂-Nb₂O₅ electrodes for electrochemical textile wastewater treatment. *Science of The Total Environment* 860: 160366.
- Trasatti S. (1991) Physical electrochemistry of ceramic oxides. *Electrochimica Acta*. 36 (2): 225-241. [https://doi.org/10.1016/0013-4686\(91\)85244-2](https://doi.org/10.1016/0013-4686(91)85244-2)

- Wafia B., Samir D. (2021) Experimental study and mathematical modeling of the corrosion inhibition of mild steel with an organic compound in 1 M HCl. *J. Electrochem. Sci. Eng.* 11 (4): 227-239. DOI: <https://doi.org/10.5599/jese.1050>
- Wen T.C., Hu C.C. (1992) Hydrogen and Oxygen Evolutions on Ru-Ir Binary Oxides. *Journal of the Electrochemical Society*, 139(8), 2158.
- Zhang J., Kwon S., Chen K., Liu X., Yang J., Sun H., Wang Y., Uchiyama T., Uchimoto Y., Li S., Li Y., Fan X., Chen G., Xia F., Wu J., Li Y., Yue Q., Qiao L., Su D., Zhou H., Goddard III W.A., Kang Y. (2025) Tantalum-stabilized ruthenium oxide electrocatalysts for industrial water electrolysis. *SCIENCE* 387 (6729), 48-55. DOI: [10.1126/science.ado9938](https://doi.org/10.1126/science.ado9938)
- Zhu C., Hao Y., Wang H., Li X., Yang Y., Ma H. (2023) Conversion of polyphenolic polymers in aerobic biochemical treatment. *Journal of Environmental Chemical Engineering*, 11(2), 109343. <https://doi.org/10.1016/j.jece.2023.109343>

(2025) ; <http://www.jmaterenvironsci.com>